

Turbulence Measurements from Five-Beam Acoustic Doppler Current Profilers

MARICARMEN GUERRA AND JIM THOMSON

Applied Physics Laboratory, University of Washington, Seattle, Washington

(Manuscript received 9 August 2016, in final form 7 March 2017)

ABSTRACT

Two new five-beam acoustic Doppler current profilers—the Nortek Signature1000 AD2CP and the Teledyne RDI Sentinel V50—are demonstrated to measure turbulence at two energetic tidal channels within Puget Sound, Washington. The quality of the raw data is tested by analyzing the turbulent kinetic energy frequency spectra, the turbulence spatial structure function, the shear in the profiles, and the covariance Reynolds stresses. The five-beam configuration allows for a direct estimation of the Reynolds stresses from along-beam velocity fluctuations. The Nortek's low Doppler noise and high sampling frequency allow for the observation of the turbulent inertial subrange in both the frequency spectra and the turbulence structure function. The turbulence parameters obtained from the five-beam acoustic Doppler current profilers are validated with turbulence data from simultaneous measurements with acoustic Doppler velocimeters. These combined results are then used to assess a turbulent kinetic energy budget in which depth profiles of the turbulent kinetic energy dissipation and production rates are compared. The associated codes are publicly available on the MATLAB File Exchange website.

1. Introduction

Acoustic Doppler current profilers (ADCPs) are commonly used to measure the horizontal components of fluid velocities along depth profiles in the ocean using three or four diverging acoustic beams. The raw data from ADCPs, termed pings, correspond to single velocity measurements in the along-beam direction. The raw ping data are typically burst averaged in time (5–10 min for tidal flows to ensure stationary mean flow conditions; [McCaffrey et al. 2015](#)). Averaging reduces the Doppler noise inherent to the measurement, which can add significant variance to the raw signals (above and beyond the variance due to real turbulent fluctuations; [Brumley et al. 1991](#)). However, if the raw along-beam velocities are retained, then many turbulence parameters, such as turbulent kinetic energy dissipation rates and Reynolds stresses, can be estimated from ADCP measurements. Estimation methods are based on the variance and correlations of the along-beam

velocity fluctuations, often with explicit removal of the variance contributed by the Doppler noise ([Lu and Lueck 1999](#); [Stacey et al. 1999](#); [Wiles et al. 2006](#); [Thomson et al. 2012](#)).

Indirect methods to estimate turbulent dissipation rates, such as turbulence kinetic energy (TKE) spectra and the turbulence structure functions ([Pope 2000](#)), are based on Kolmogorov's hypothesis about the existence of a range of turbulent length scales within the isotropic turbulence energy cascade, known as inertial subrange, in which the energy transfer is solely determined by the dissipation rate ([Kolmogorov 1941](#); [Pope 2000](#)). The application of these methods requires observing the inertial subrange in the data ([Pope 2000](#)).

In the frequency domain, some authors (e.g., [Thomson et al. 2012](#); [Richard et al. 2013](#); [Durgesh et al. 2014](#)) have attempted to use spectra calculated from raw along-beam velocity ADCP data, but the inherent Doppler noise typically obscures the inertial subrange ([Richard et al. 2013](#)). Recently, turbulence dissipation rates have been estimated from turbulence spectra after averaging the frequency spectra for different mean flows and bins in order to successfully observe the inertial subrange in the turbulence energy cascade in [McMillan et al. \(2016\)](#) and

 Denotes content that is immediately available upon publication as open access.

Corresponding author: Maricarmen Guerra, mguerrap@uw.edu

McMillan and Hay (2017). Another common technique is to estimate turbulent dissipation rates using the second-order spatial structure function of turbulence (Wiles et al. 2006; Rusello and Cowen 2011).

One of the most frequently used techniques to estimate Reynolds stresses from ADCP along-beam velocities is the variance technique (Lu and Lueck 1999; Stacey et al. 1999; Rippeth et al. 2003), which provides two components (out of six) of the Reynolds stresses and is based on the variance of opposite beam velocity fluctuations.

A new generation of broadband five-beam ADCPs with the ability to measure flow velocity at higher frequencies and with lower noise levels is poised to expand routine turbulence measurements. Moreover, the inclusion of a fifth beam allows for a true measurement of vertical velocities and the estimation of five (out of six) Reynolds stresses, total TKE, and anisotropy directly from the along-beam velocities (Lu and Lueck 1999; R. Dewey and S. Stringer 2007, unpublished manuscript). This is a notable expansion beyond the four-beam variance methods (Lu and Lueck 1999; Stacey et al. 1999; Rippeth et al. 2003). These new features, together with the integration of inertial motion units, might even expand the application of these ADCPs to the study of upper-ocean turbulence and wave-breaking turbulence, and to improve the estimation of parameters used in turbulence models.

This paper presents turbulence measurements from two new five-beam acoustic current profilers: the Nortek Signature1000 (kHz), which uses the acronym AD2CP to distinguish it from the previous generation of profilers, and the new Teledyne RDI Sentinel V50 500 (kHz). The new instruments' capabilities are assessed in two field deployments in highly energetic tidal channels, calculations of turbulence parameters, and the subsequent evaluation of TKE budgets.

The results are validated using measurements from acoustic Doppler velocimeters (ADV), which are typically the preferred choice for turbulence measurements. However, ADVs only measure at a point, and their deployment at middepths requires complicated moorings and subsequent motion corrections to the raw data (Thomson et al. 2013). The new ADCPs are shown to be a more practical alternative to ADVs, with the potential for new insights about where turbulence is being produced and dissipated in the water column.

In section 2 details of the field measurements are presented. In section 3, estimates of the TKE dissipation rate are presented using two different methods: the TKE frequency spectra and the second-order spatial structure function. In section 4, the terms of the TKE production

rate are estimated; in particular, Reynolds stresses are calculated using along-beam velocities from all five beams. Finally, in section 5, the TKE dissipation and production rate estimates are used to examine the TKE budget at the two tidal channels.

2. Data collection

a. Site description

Turbulence measurements were taken at Admiralty Inlet and Rich Passage, two tidal channels located in Puget Sound, Washington. Figure 1a shows the location of the field sites and the detailed locations of the instruments. A summary of the deployments and instrument settings is presented in Table 1.

Admiralty Inlet is located in the northern part of Puget Sound (48.14°N, 122.71°W). Admiralty Inlet is ~6.5 km wide and ~50 m deep at the measurement site. The principal direction of the flow is ~50° from the east in the clockwise direction.

Rich Passage is located south of Bainbridge Island in Puget Sound (47.59°N, 122.56°W). At the measurements site the channel is ~24 m deep and ~550 m wide. The channel is oriented ~45° from north in the clockwise direction.

b. Instruments and settings

The five-beam Doppler profilers were deployed mounted looking upward on separate Oceanscience Sea Spider tripods, which place each instrument ~0.9 m above the seafloor when deployed. The instruments have four beams slanted at 25° from the vertical, plus a fifth vertical beam. Deployments were on 11 May 2015 at Admiralty Inlet and on May 17–18 2015 at Rich Passage. Table 1 summarizes the deployments and sampling parameters.

The Nortek Signature was configured to measure turbulence in along-beam coordinates using its five beams at 8 Hz (the maximum possible when using all five beams) for bursts lasting 10 min in duration. At Admiralty Inlet, the interval between bursts was 20 min and there were 20 velocity bins at 1-m spacing. At Rich Passage, the interval between bursts was 30 min and there were 15 velocity bins at 1-m spacing.

The Teledyne RDI Sentinel V50 was configured to measure along-beam turbulent velocities at 2 Hz (the maximum possible when using all five beams) for 10-min bursts with a 20-min interval. At Admiralty Inlet, the RDI Sentinel V50 tripod was ~80 m away from the Nortek Signature tripod and there were 20 velocity bins at 1-m spacing. At Rich Passage, the Sentinel V50 was not deployed (it was unavailable).

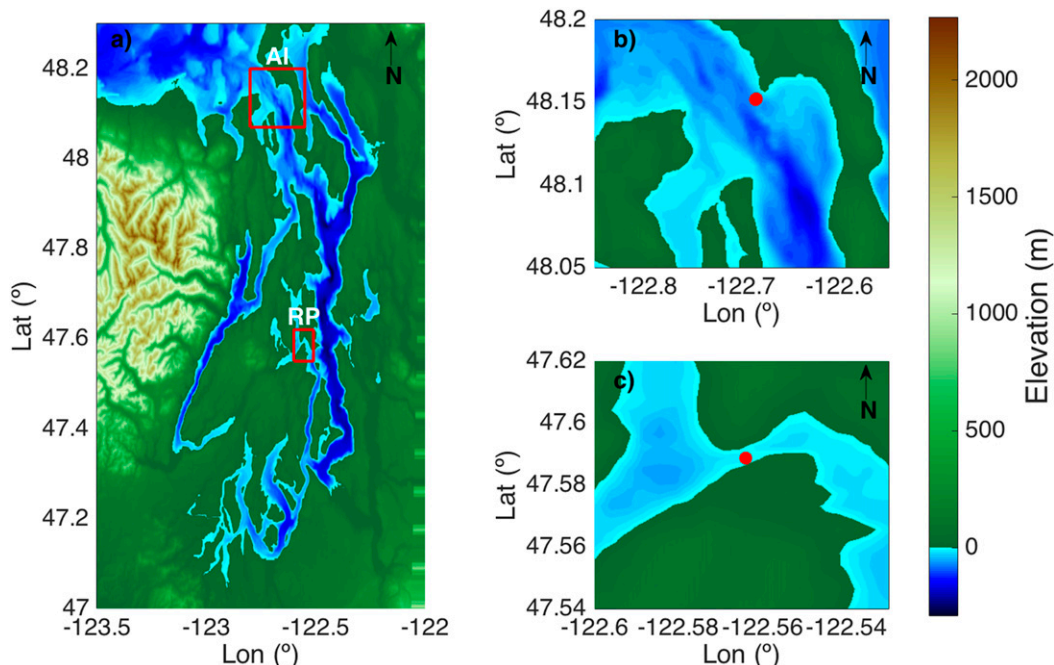


FIG. 1. Bathymetry and location of the two tidal channels: (a) Puget Sound, (b) Admiralty Inlet (AI), and (c) Rich Passage (RP). Red dots indicate the locations of the instruments.

In addition to the two five-beam acoustic Doppler current profilers, ADVs were deployed at both sites in the vicinity of the instruments in order to compare and validate the data from the profilers.

At Admiralty Inlet, a Nortek Vector ADV was deployed 130 m east of the Nortek Signature on board a tidal turbulence mooring (TTM; Thomson et al. 2013; Harding et al. 2017; Kilcher et al. 2017) on 11–13 May 2015. The TTM consists of an anchor (~1000-kg wet weight) to hold the mooring in place, a

sphere (~300-kg positive buoyancy) to hold the mooring vertical, and an instrumentation vane inline between the anchor and the buoy where the ADV was mounted. The TTM positions the ADV at 10 m above the sea bottom. The ADV was set to measure velocities at 16 Hz continuously. An inertial motion unit (IMU) synchronously measured TTM acceleration and orientation; these data are used to remove contaminations of mooring motion from the ADV turbulent velocities. The motion correction method is

TABLE 1. Summary of deployments and sampling parameters at Admiralty Inlet and Rich Passage.

Location	Admiralty Inlet	Admiralty Inlet	Admiralty Inlet	Rich Passage	Rich Passage
Instrument	Nortek Signature1000	RDI Sentinel V50	Nortek Vector ADV	Nortek Signature1000	Nortek Vector ADV
Latitude (°)	48.1522	48.1517	48.1524	47.5887	47.5887
Longitude (°)	-122.6852	-122.6858	-122.6868	-122.5641	-122.5641
Water depth (m)	50	50	50	24	24
Deployment duration (days)	2	2	2	2	0.1
Sampling frequency (Hz)	8	2	16	8	16
Burst average (min)	10	10	10	10	10
Δz (m)	1	1	—	1	—
Distance to first cell (m)	0.5	0.5	—	0.5	—
Range (m)	20.5	20.5	—	15.5	—
z target (m)	—	—	10	—	17
Single-ping error ($m s^{-1}$)	0.016	0.003	0.02	0.016	0.02
Empirical error ($m s^{-1}$)	0.027	0.054	0.011	0.027	0.011
Pitch (°)	2.26 ± 0.005	4.45 ± 0.06	—	0.35 ± 0.002	—
Roll (°)	0.36 ± 0.02	-1.61 ± 0.01	—	-1.19 ± 0.004	—

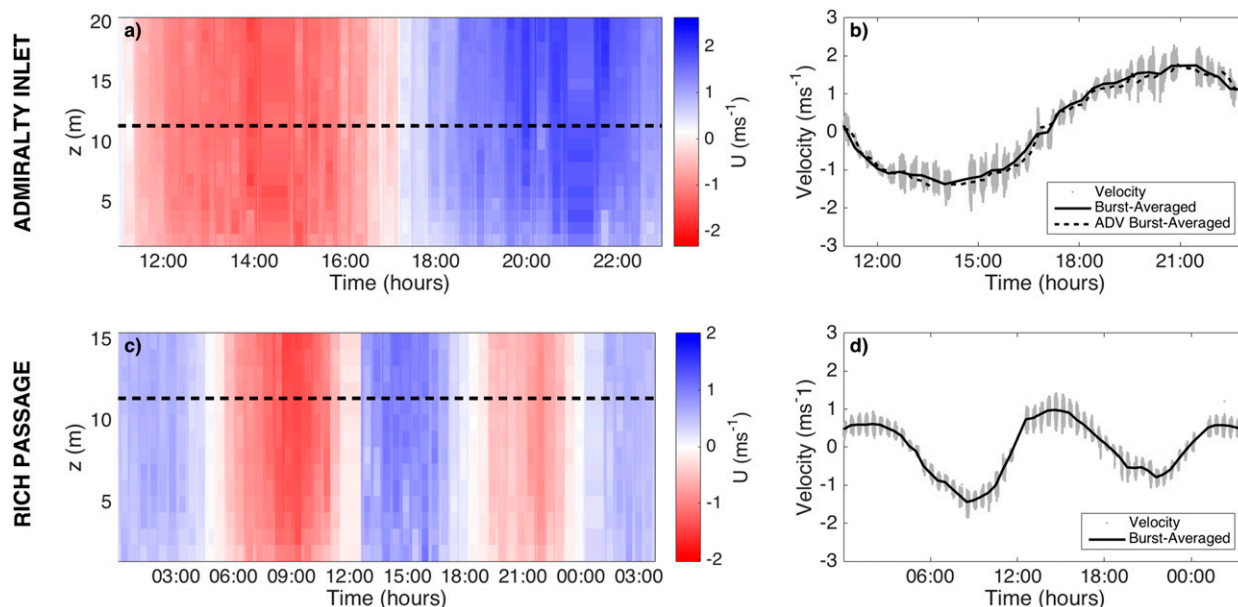


FIG. 2. Vertical profiles and time series of along-channel velocities measured with the Nortek Signature at (a),(b) Admiralty Inlet and (c),(d) Rich Passage. In (a) and (c), black dashed line indicates depth corresponding to the time series (as $z = 10.4$ m from sea bottom). In (b) and (d), gray dots correspond to measured along-channel velocity, and black line corresponds to 10-min burst-averaged along-channel velocity. Burst-averaged along-channel velocity measured with the TTM ADV at Admiralty Inlet is included as a black dashed line in (b).

described in detail in Thomson et al. (2013) and Kilcher et al. (2017).

At Rich Passage, a Nortek Vector ADV was deployed in the same location as the Nortek Signature. The ADV was mounted on a turbulence torpedo (TT), a sounding weight that hangs from a davit on the side of the ship while the ship is holding station (Thomson et al. 2013; Harding et al. 2017; Kilcher et al. 2017). The turbulence torpedo ADV was deployed on 5 June 2015, sampling turbulent velocities at 16 Hz for 2.5 h during ebb tide (mean flow ranging between 1.5 and 2 m s^{-1}). Motion corrections were applied to the velocity measurements following the same methods used for the TTM ADV measurements (Thomson et al. 2013; Kilcher et al. 2017).

c. Raw data

Figure 2 shows vertical profiles, and time series, of the along-channel velocity (after a coordinate transformation of the beam velocities) measured by the Nortek Signature for both study sites. At Admiralty Inlet, it was possible to measure only a single tidal cycle due to the rapid battery consumption when sampling at high frequency and not using external battery canisters. After approximately 12 h, the Nortek Signature kept sampling, but the bursts became shorter (less than the 10-min setting). At Rich Passage, a reduced duty cycle made it possible to measure two tidal

cycles before the bursts became shorter. For both deployments, a single battery pack was used, but additional battery packs can be externally connected to the instrument to overcome the limits from rapid battery consumption. According to the Nortek Signature Deployment software, for a deployment using the same settings as for the Admiralty Inlet Signature deployment, the instrument life can be extended to 158 days when using a 3600-Wh lithium external battery pack. For the same deployment settings, a memory card with 64-GB capacity would last 179.5 days (and thereby exceed the limitations of the external batteries).

A 10-min time interval is selected for burst averaging these datasets and for estimating statistical parameters (spectra, structure function, etc.). This time interval is chosen as short enough to remove any trend contamination from tidal currents in the turbulence time series (i.e., short enough so that the tidal current does not change) but long enough to capture the large-scale turbulence (McCaffrey et al. 2015). An analysis of this time interval selection for turbulence analysis in tidal channels is available in McCaffrey et al. (2015).

The maximum observed burst-averaged horizontal speed at Admiralty Inlet was 2.04 m s^{-1} during flood, which corresponds to a Reynolds number of $O(10^8)$. At Rich Passage the maximum burst-averaged observed

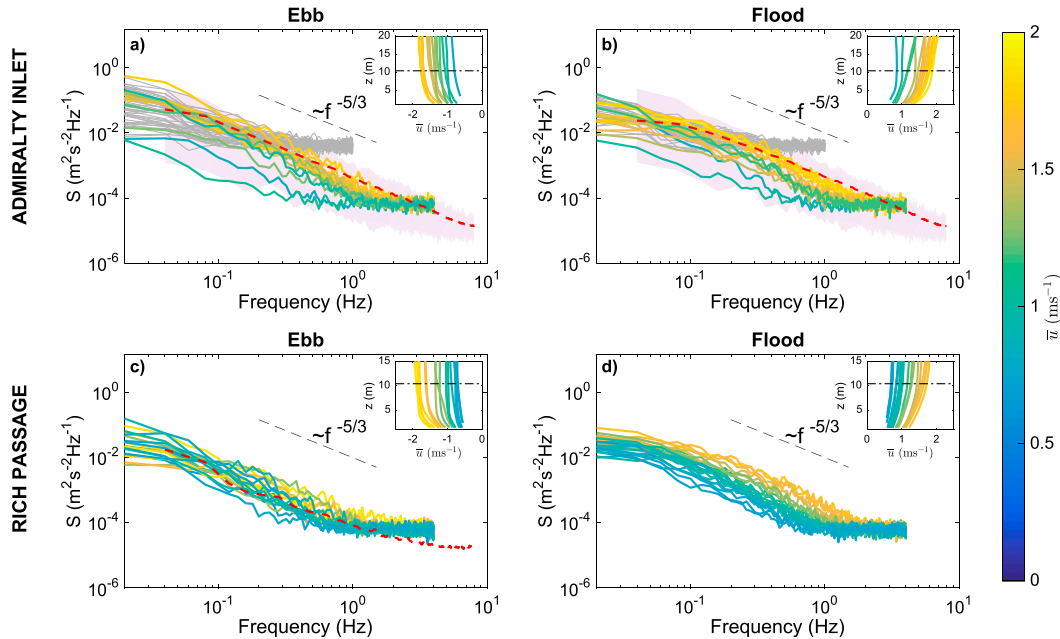


FIG. 3. TKE spectra at $z = 10.4$ m for different mean flows (by color) at (a),(b) Admiralty Inlet and (c), (d) Rich Passage. Dashed black line is proportional to $f^{-5/3}$. Inset plots show burst-averaged horizontal speed vertical profiles (also by color); dotted-dashed line shows $z = 10.4$ m in the profiles. In the Admiralty Inlet plots, spectra from the RDI Sentinel V50 data are included as gray curves, and the range of spectra from the TTM ADV data is included as a light pink area. Dashed red line corresponds to averaged spectra from ADV data.

horizontal speed was 1.95 m s^{-1} during ebb, which corresponds to a Reynolds number of $O(10^7)$. Although these are short datasets, they are sufficient to observe turbulent velocity fluctuations at a wide range of mean flow conditions at each site (e.g., 10-min burst-averaged horizontal speeds varied from 0 to 2 m s^{-1}). Data are quality controlled to remove measurements with low beam correlations (less than 50) and low echo amplitude (less than 30 dB), as per manufacturer recommendation. This removes a very small fraction (less than 0.5%) of the raw data.

3. Turbulent kinetic energy dissipation rate

At each depth in the ADCPs’ measured profiles, the TKE dissipation rate is estimated by two methodologies: from the frequency spectra (Lumley and Terray 1983) and from the spatial structure function (Wiles et al. 2006). Both methods are derived from Kolmogorov’s turbulence hypotheses (Kolmogorov 1941; Pope 2000) and require the observation of the inertial subrange of isotropic turbulence.

a. Turbulent kinetic energy spectra

The distribution of turbulent kinetic energy among eddies of different sizes is represented through the

turbulent kinetic energy spectra. Assuming stationarity, the turbulence advected past the instruments at average speeds \bar{u} has frequency f spectra that are related to the wavenumber k spectra by $\bar{u} \propto f/k$ (i.e., Taylor’s frozen field). Thus, the frequency spectra are expected to include an inertial subrange in which the turbulent kinetic energy follows $f^{-5/3}$ as a manifestation of the energy cascade following $k^{-5/3}$ (Kolmogorov 1941; Pope 2000).

TKE spectra are estimated using Welch’s overlapped segment averaging method applied to the vertical beam velocities (beam 5). For the Nortek Signature datasets, spectral estimates are calculated for every 10-min burst using twenty-three 50-s sub-windows with 50% overlap and a Hanning data taper, which results in an ensemble spectral density estimate with ~ 45 degrees of freedom. TKE spectra with the same degrees of freedom are also estimated for the RDI Sentinel V50 vertical beam velocities and for the Nortek Vector ADV measurements.

TKE spectra estimates for both sites for the tenth vertical bin (10.4 m from the sea bottom) are presented in Fig. 3 colored by mean flow conditions. The TKE spectra estimates from the RDI Sentinel V50 measurements for the same bin are included in the Admiralty Inlet figures in gray. Averaged TKE spectra from the Nortek Vector ADV data are included for comparison

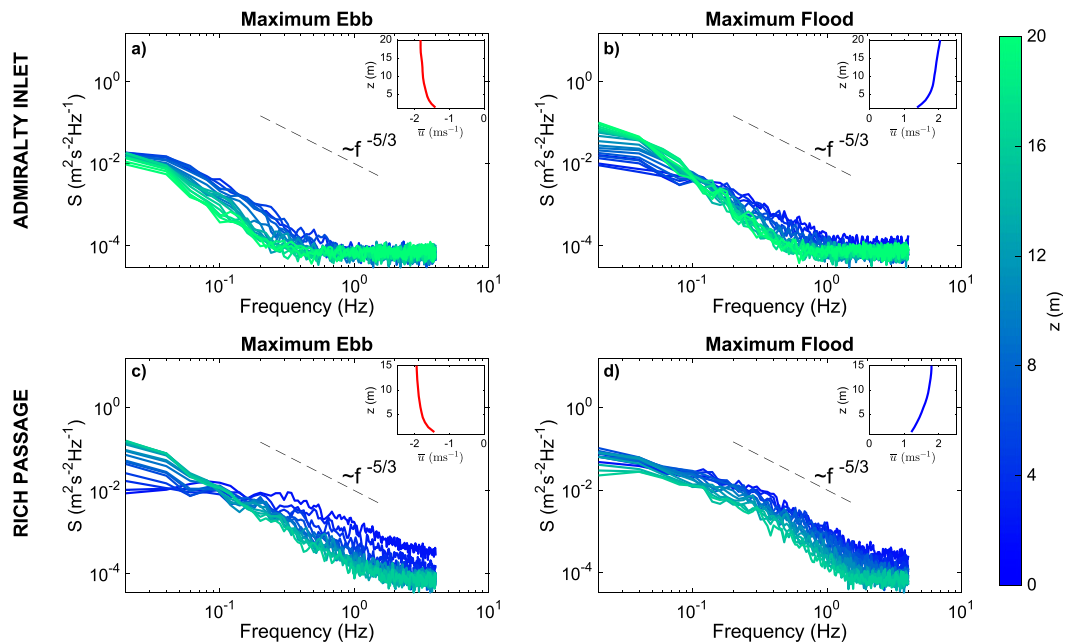


FIG. 4. TKE spectra at maximum ebb and flood mean flow conditions at different depths (by color) at (a),(b) Admiralty Inlet and (c),(d) Rich Passage. Dashed black line is proportional to $f^{-5/3}$. Inset plots show corresponding mean flow vertical profile.

as a red dashed line when available; the range of TKE spectra from the TTM ADV data is included as a pink area in the Admiralty Inlet plots. In this analysis, mean flows that are close to slack conditions ($\bar{u} < 0.5 \text{ m s}^{-1}$) have been removed, as the spectra do not show the theoretical $f^{-5/3}$ slope. Spectral density estimates from the Nortek Signature data are generally well sorted by mean flow velocity, implying that a higher TKE is observed at higher mean flows. The exception is during the stronger ebb at Rich Passage, where the instrument is in the lee of a sill.

The most novel result from the Nortek Signature data is the clear observation of the TKE energy cascade in the spectral estimates, which is usually obscured by the Doppler noise of profiling instruments. An isotropic region of tridimensional turbulence is present at midfrequencies ($0.1 < f < 1 \text{ Hz}$), which follows the classic $f^{-5/3}$ energy cascade (Kolmogorov 1941). At higher ($f > 1 \text{ Hz}$) frequencies, the spectra become affected by the instrument inherent Doppler noise. The spectral noise level of the Nortek Signature is observed around $S_w(f) = 10^{-4} \text{ m}^2 \text{ s}^{-2} \text{ Hz}^{-1}$, while the noise level of the Nortek Vector is observed around $S_w(f) = 10^{-5} \text{ m}^2 \text{ s}^{-2} \text{ Hz}^{-1}$. The noise level of the RDI Sentinel V50, by contrast, is much higher at $S_w(f) = 10^{-2} \text{ m}^2 \text{ s}^{-2} \text{ Hz}^{-1}$, and thus the inertial subrange is typically obscured in those spectra.

The lower spectral noise floor observed from the Nortek Signature data might be attributed to its ability

to sample faster. Even if the single-ping error were the same between the RDI Sentinel V50 and the Nortek Signature, the noise floor observed in a spectral density will still be lower when the sampling is faster, as it is redistributed along a wider frequency range. To fairly compare the observed spectral noise floor of the two profilers, the data from the Nortek Signature is subsampled down to 2 Hz and new spectra are estimated (but not shown). For the subsampled case, the TKE energy cascade is still observed between $0.1 < f < 0.8 \text{ Hz}$, and the noise level is observed around $S_w(f) = 2 \times 10^{-4} \text{ m}^2 \text{ s}^{-2} \text{ Hz}^{-1}$. This is slightly higher than when sampling at 8 Hz but not nearly as high as the spectral noise level of the RDI. The latter implies that even when sampling at the same frequency, the Nortek Signature presents a lower Doppler noise. The higher noise level of the RDI Sentinel V50 data obscures the inertial subrange in these TKE spectra, preventing the following estimation of the TKE dissipation rate.

Figure 4 shows spectral estimates at maximum ebb and flood at the two sites for all vertical bins from the Nortek Signature data. The spectral estimates are well sorted by depth, except for the maximum ebb at Rich Passage due to the existence of a vertical sill upstream of the measurement location. TKE density decreases as the distance from the bottom increases, consistent with bottom-generated turbulence. In the higher bins, the observable portion of the inertial subrange becomes

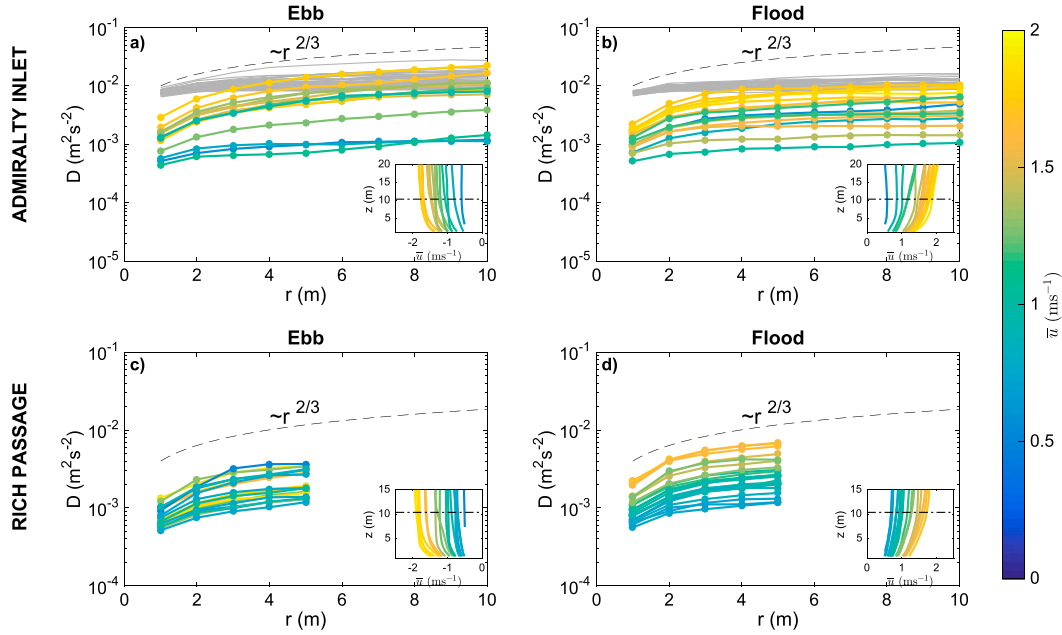


FIG. 5. Spatial structure function at $z = 10.4$ m for different mean flows (by color) at (a), (b) Admiralty Inlet and (c), (d) Rich Passage. The dashed line is proportional to $r^{2/3}$. Inset plots show mean flow vertical profiles (also by color); the dotted–dashed line corresponds to $z = 10.4$ m. In the Admiralty Inlet plots, structure functions from the RDI Sentinel V50 data are included as gray curves.

narrower due to the decrease in TKE density (i.e., the noise floor affects spectra at a lower frequency); for example, at 20.4 m from the sea bottom, the inertial subrange is observed at $0.1 < f < 0.6$ Hz.

The dissipation rate of TKE ε is related to the isotropic portion of the vertical TKE frequency spectrum by

$$S_w(f) = \alpha \varepsilon^{2/3} f^{-5/3} \left(\frac{\bar{u}}{2\pi} \right)^{2/3}, \quad (1)$$

where α is a constant equal to 0.69 (Sreenivasan 1995), ε is the TKE dissipation rate, f is the frequency, and \bar{u} is the mean along-channel velocity. This applies Taylor’s “frozen field hypothesis,” which assumes that the turbulence is in steady state as it advects past the instrument (neither developing nor decaying), such that we can transform the temporal observation into a spatial one (i.e., $f = \bar{u}k/2\pi$, where k is the spatial wavenumber).

Each estimated spectrum is multiplied by $f^{5/3}$ to obtain a compensated spectrum, which should be horizontal (flat) in the presence of an inertial subrange. The dissipation rate is estimated by solving $S_w(f) f^{5/3} |_{f_1}^{f_2} = \alpha \varepsilon^{2/3} (\bar{u}/2\pi)^{2/3}$, where f_1 – f_2 is the frequency range with the slope closest to zero in the compensated spectra. The range of frequencies used to estimate the mean compensated spectra, $S_w(f) f^{5/3}$, varies according

to the position of the inertial subrange for different mean flows and depths, ranging between $0.1 < f < 1$ Hz. A minimum of five frequencies are used to estimate dissipation rates from the compensated spectra.

Uncertainties in the TKE dissipation rates from spectra are calculated by propagating the uncertainty in the compensated spectra (Bassett et al. 2013), such that

$$\sigma_{\varepsilon_s} = \frac{2\pi}{\bar{u}} \left(\frac{1}{\alpha} \right)^{3/2} \frac{3}{2} S_{w_{\text{comp}}}^{-1/2} \sigma_{S_{w_{\text{comp}}}}, \quad (2)$$

where σ_{ε_s} is the uncertainty in the dissipation rate estimate and $\sigma_{S_{w_{\text{comp}}}}$ is taken to be the variance of the compensated spectra in the range of frequencies used to estimate ε .

b. Turbulence structure function

The along-beam velocities can be used to estimate the second-order spatial structure function of the along-beam turbulent fluctuations, $D(z, r)$, following the methodology described in Wiles et al. (2006). The structure function is defined as

$$D_i(z, r) = \langle [u'_i(z+r) - u'_i(z)]^2 \rangle, \quad (3)$$

where z is the along-beam measurement location, u'_i corresponds to each along-beam velocity fluctuation, and r is the distance between two velocity bins; the

angle brackets denote a time average over the burst (10-min bursts for these datasets).

The structure function $D_i(z, r)$ is estimated from the bottom of the profile upward. The distance r is set to be positive and is limited by the distance to the closest boundary, which in these cases is the sea bottom. Figure 5 shows examples of the spatial structure function for the vertical beam turbulent fluctuations, $D_5(z, r)$, at $z = 10.4$ m from the sea bottom at both sites. The structure function estimates from the RDI Sentinel V50 measurements for the same bin are included in the Admiralty Inlet figures in gray. Structure functions from the Nortek Signature data are generally well sorted by the mean flow, except during the stronger ebb at Rich Passage, where again the sill creates a region of low turbulence. The slopes of the structure functions from the Nortek Signature agree well with the expected $r^{2/3}$ at both sites. Again, it is not possible to observe the theoretical $r^{2/3}$ slope in the structure function estimates from the RDI Sentinel V50. The structure function offset at $r = 0$, N , is related to the instrument Doppler noise, σ_N , as $N = 2 \times \sigma_N$ (Wiles et al. 2006; Thomson 2012). A higher offset N is observed in the RDI Sentinel V50 structure functions due to its higher Doppler noise, which prevents the structure function drop-off as r approaches zero, obscuring the $r^{2/3}$ slope, and thus limiting the estimation of the TKE dissipation rate. In these measurements, the 1-m bin size limits the observed turbulence length scales and particularly affects the observation of the inertial subrange in the turbulence structure function (McMillan and Hay 2017).

In the inertial subrange, the structure function is related to r and ε by

$$D_i(z, r) = C_v^2 \varepsilon^{2/3} r^{2/3}, \quad (4)$$

where C_v^2 is a constant equal to 2.1 (Wiles et al. 2006; Thomson et al. 2012).

The structure function is multiplied by $r^{-2/3}$ to obtain a compensated structure function in the inertial subrange (Rusello and Cowen 2011). The dissipation rate is estimated by solving $\overline{D(z, r)r^{-2/3}}|_{r_1}^{r_2} = C_v^2 \varepsilon^{2/3}$, where r_1 – r_2 is the range with the slope closest to zero. Estimates are not calculated for depths with fewer than four points in the structure function. At Admiralty Inlet, the minimum r range used in the estimates is 1–4 m and the maximum range is 1–10 m; at Rich Passage the minimum range is 1–4 m and the maximum range is 1–7 m. Within the valid depths, the structure function is quality controlled to remove estimates with negative slope, resulting in a loss of 21% of valid structure functions at Admiralty Inlet and 28% at Rich Passage, for which no dissipation estimate is available. Although this is a rather severe

amount of quality control, it is less than that of other studies applying the structure function (McMillan et al. 2016; Thomson 2012).

Uncertainties in TKE dissipation rates from the structure function fitting are calculated by propagating the uncertainty in the compensated structure function, such that

$$\sigma_{\varepsilon_D} = \left(\frac{1}{C_v^2} \right)^{3/2} \frac{3}{2} \overline{D}_{\text{comp}}^{-1/2} \sigma_{D_{\text{comp}}}, \quad (5)$$

where σ_{ε_D} is the uncertainty in the dissipation rate estimate, and $\sigma_{D_{\text{comp}}}$ is taken to be the variance of the compensated structure function in the range of bin separations used to estimate ε .

Figure 6 shows averaged vertical profiles of TKE dissipation rates, separated by ebb and flood tides, with their corresponding error estimates for both sites and compares the two methods. The TKE dissipation rate estimates from the two methods are in agreement, although the estimates from the structure function do not cover the entire measured profile due to the r limitation. AD2CP TKE dissipation rate estimates are also in good agreement with estimates from ADV data, even at Rich Passage, where the TT ADV was located above the top of the profile measured by the Nortek Signature. Averaged uncertainties, expressed as a percentage of the flood/ebb averaged TKE dissipation rates, present different patterns at each site. At Admiralty Inlet, uncertainties from the structure function range between 12%, closer to the bottom, and 22%, higher in the water column. At Rich Passage, uncertainties from the structure function method remain between 10% and 15% through the water column, while uncertainties from the TKE spectra method range between the 15%, closer to the bottom, and 25% higher in the water column.

4. Turbulent kinetic energy production rate

In a well-mixed environment, the buoyancy TKE sink term can be neglected, and the TKE is primarily produced by the mean flow shear. If the horizontal shear is small, then the TKE production can be approximated in terms of the Reynolds stresses and the velocity vertical gradients as

$$P = -\overline{u'_{\text{ch}} w'} \frac{\partial \overline{u}_{\text{ch}}}{\partial z} - \overline{v'_{\text{ch}} w'} \frac{\partial \overline{v}_{\text{ch}}}{\partial z} - \overline{w' w'} \frac{\partial \overline{w}}{\partial z}, \quad (6)$$

where P is the production of TKE; u_{ch} , v_{ch} , and w are the along-channel, across-channel, and vertical velocities respectively; and the primes denote velocity fluctuations.

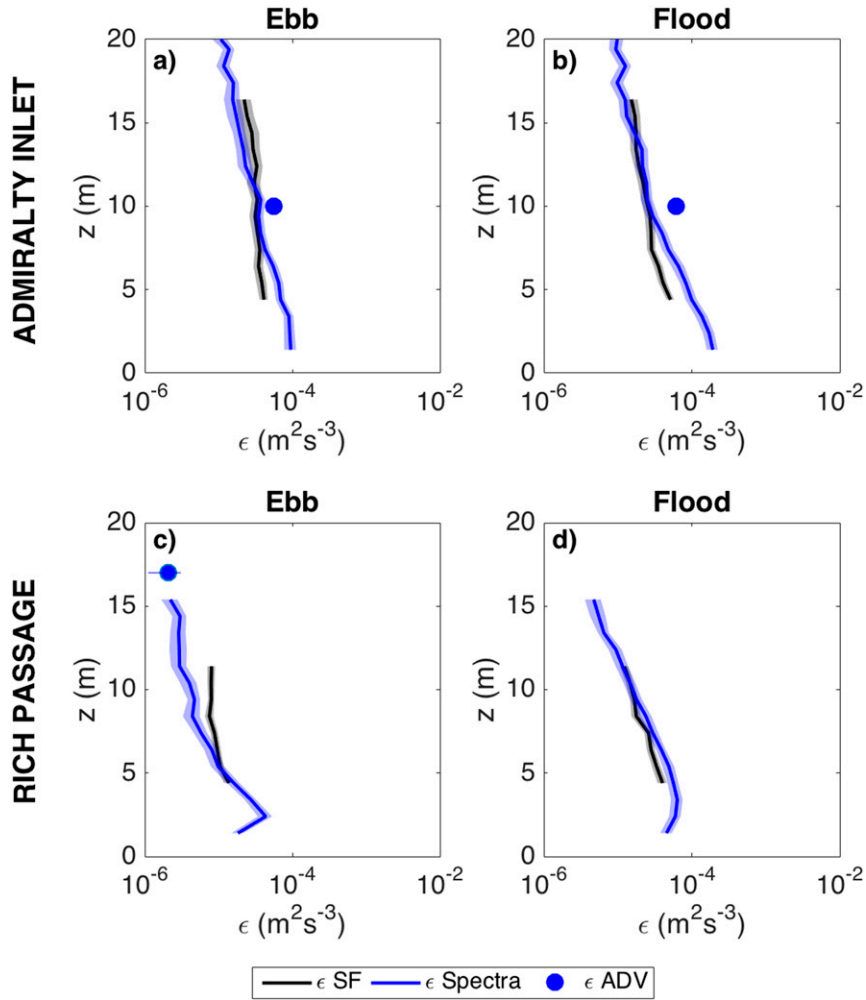


FIG. 6. Average vertical profiles of TKE dissipation rate at (a),(b) Admiralty Inlet and (c),(d) Rich Passage, from TKE spectra (blue line) and turbulence structure function (black line). TKE dissipation rate estimates from the TTM ADV spectra (blue dots).

a. Vertical shear

Along-beam velocities are transformed into orthogonal east–north–up components. The horizontal components are rotated to obtain along- and across-channel velocity components at each location. The vertical gradients of the along-channel, across-channel, and vertical velocities, $\partial \overline{u}_{ch}/\partial z$, $\partial \overline{v}_{ch}/\partial z$, $\partial \overline{w}/\partial z$, respectively, are estimated as the centered difference of their burst average using the vertical distance between measurements.

The uncertainty in the shear estimations is calculated following Williams and Simpson (2004) method as

$$\sigma_S^2 = \frac{\sigma_N^2}{M \Delta z^2 \sin^2 2\theta}, \tag{7}$$

where σ_N is the instrument inherent Doppler noise, M is the number of samples used in the burst average,

and θ is the beam inclination angle. This estimate corresponds to the minimum level of shear detection considering only instrument noise as a source of error in the measurements (Williams and Simpson 2004). It has been previously reported that instrument noise from instrument software is usually biased low (Williams and Simpson 2004; Thomson et al. 2012). In this study, the instrument noise is estimated from the spectral noise level, as it is considered to be white noise (i.e., has a constant horizontal spectra; McMillan and Hay 2017). The estimated ping-to-ping instrument noise levels from spectra are $\sigma_N = 2.65 \text{ cm s}^{-1}$ for the Nortek Signature, and $\sigma_N = 5.39 \text{ cm s}^{-1}$ for the RDI Sentinel V50. Instrument noise reported by the instruments’ corresponding software for each deployment and empirically estimated noise are shown in Table 1.

b. Reynolds stresses

The Reynolds stress tensor is estimated following the methodology of R. Dewey and S. Stringer (2007, unpublished manuscript) for a five-beam ADCP configuration. This methodology extends the variance technique (Lu and Lueck 1999; Stacey et al. 1999; Rippeth et al. 2003) to different ADCP beam configurations, including expressions for the Reynolds stresses for nonzero tilt. The use of five beams allows for exact expressions for five of the Reynolds stresses, total TKE, and anisotropy (R. Dewey and S. Stringer 2007, unpublished manuscript). This method assumes small angle approximations for pitch and roll, which were achieved in these deployments (mean pitch $\sim 2.3^\circ$ and mean roll $\sim 0.4^\circ$ at Admiralty Inlet, mean pitch $\sim 0.35^\circ$ and mean roll approximately -1.19° at Rich Passage). The Reynolds stresses from R. Dewey and S. Stringer (2007, unpublished manuscript) are written in instrument coordinates (assuming heading is equal to zero); thus, the obtained stresses are rotated to along- and across-channel coordinates after the calculations.

The following equations, from R. Dewey and S. Stringer (2007, unpublished manuscript), define the Reynolds stresses in instrument coordinates for any five-beam ADCP, assuming small tilt angle approximation:

$$\overline{u^2} = \frac{-1}{4 \sin^6 \theta \cos^2 \theta} [-2 \sin^4 \theta \cos^2 \theta (\overline{u_2^2} + \overline{u_1^2} - 2 \cos^2 \theta \overline{u_5^2}) + 2 \sin^5 \theta \cos \theta \phi_3 (\overline{u_2^2} - \overline{u_1^2})], \quad (8)$$

$$\overline{v^2} = \frac{-1}{4 \sin^6 \theta \cos^2 \theta} [-2 \sin^4 \theta \cos^2 \theta (\overline{u_4^2} + \overline{u_3^2} - 2 \cos^2 \theta \overline{u_5^2}) - 2 \sin^4 \theta \cos^2 \theta \phi_3 (\overline{u_2^2} - \overline{u_1^2}) + 2 \sin^3 \theta \cos^3 \theta \phi_3 (\overline{u_2^2} - \overline{u_1^2}) - 2 \sin^5 \theta \cos \theta \phi_2 (\overline{u_4^2} - \overline{u_3^2})], \quad (9)$$

$$\overline{w^2} = \frac{-1}{4 \sin^6 \theta \cos^2 \theta} \{-2 \sin^5 \theta \cos \theta \phi_3 [\overline{u_2^2} - \overline{u_1^2}] + 2 \sin^5 \theta \cos \theta \phi_2 (\overline{u_4^2} - \overline{u_3^2}) - 4 \sin^6 \theta \cos^2 \theta \overline{u_5^2}\}, \quad (10)$$

$$\overline{u'w'} = \frac{-1}{4 \sin^6 \theta \cos^2 \theta} [\sin^5 \theta \cos \theta (\overline{u_2^2} - \overline{u_1^2}) + 2 \sin^4 \theta \cos^2 \theta \phi_3 (\overline{u_2^2} + \overline{u_1^2}) - 4 \sin^4 \theta \cos^2 \theta \phi_3 \overline{u_5^2} - 4 \sin^6 \theta \cos^2 \theta \phi_2 \overline{u'v'}], \quad (11)$$

$$\overline{v'w'} = \frac{-1}{4 \sin^6 \theta \cos^2 \theta} [\sin^5 \theta \cos \theta (\overline{u_4^2} - \overline{u_3^2}) - 2 \sin^4 \theta \cos^2 \theta \phi_2 (\overline{u_4^2} + \overline{u_3^2}) + 4 \sin^4 \theta \cos^2 \theta \phi_2 \overline{u_5^2} + 4 \sin^6 \theta \cos^2 \theta \phi_3 \overline{u'v'}], \quad (12)$$

where θ is the beam inclination angle (25° in these cases); ϕ_2 and ϕ_3 correspond to Dewey's pitch and roll, respectively; and $\overline{u_i^2}$ are the along-beam velocity fluctuation variances. For the Nortek Signature configuration: ϕ_2

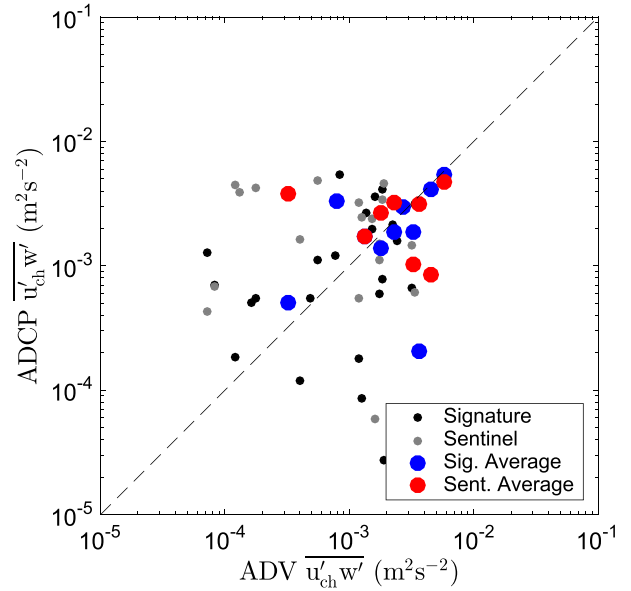


FIG. 7. Vertical shear Reynolds stress ($\overline{u'_{ch} w'}$) at Admiralty Inlet: from TTM ADV data (x axis), and from Nortek Signature and RDI Sentinel V50 estimated using R. Dewey and S. Stringer (2007, unpublished manuscript) five-beam method (y axis). Averages binned by $\overline{u'_{ch} w'}$ from the TTM ADV measurements (blue and red dots); $y = x$ (black dashed line). Averaged data correlation coefficients: 0.6 (Nortek Signature to TTM ADV), 0.05 (RDI Sentinel V50 to TTM ADV).

corresponds to roll and ϕ_3 corresponds to negative pitch, and $u_1 = u_{1\text{Sig}}$, $u_2 = u_{3\text{Sig}}$, $u_3 = u_{4\text{Sig}}$, and $u_4 = u_{2\text{Sig}}$. For the RDI Sentinel V50: ϕ_2 corresponds to pitch and ϕ_3 corresponds to roll, and $u_1 = u_{1\text{Sent}}$, $u_2 = u_{2\text{Sent}}$, $u_3 = u_{3\text{Sent}}$, and $u_4 = u_{4\text{Sent}}$.

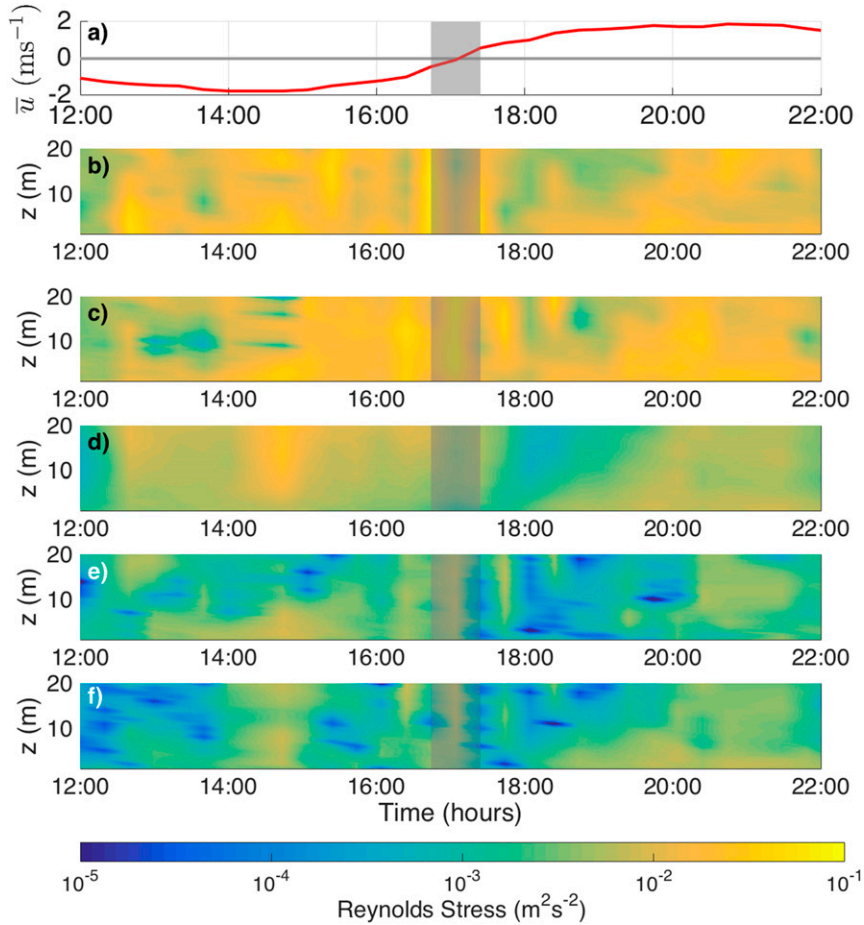


FIG. 8. Horizontal burst-averaged speed and vertical profiles of Reynolds stresses in time estimated using R. Dewey and S. Stringer (2007, unpublished manuscript) five-beam method at Admiralty Inlet: (a) mean flow, (b) $\overline{u'^2_{ch}}$, (c) $\overline{v'^2_{ch}}$, (d) $\overline{w'^2}$, (e) $\overline{u'_{ch}w'}$, and (f) $\overline{v'_{ch}w'}$. Slack conditions are marked in gray.

The Reynolds stress tensors are quality controlled to be a positive definite matrix. A total of 12% of the Reynolds stress tensors at Admiralty Inlet, and 8% at Rich Passage, do not meet this requirement.

The uncertainty in the Reynolds stress estimations is calculated following the Williams and Simpson (2004) method,

$$\sigma_{RS}^2 = \frac{\sigma_N^4}{M \sin^2 2\theta}, \quad (13)$$

where σ_N is the instrument noise, M is the number of samples used in the averaging, and θ is the beam inclination angle. This uncertainty estimate corresponds to the minimum level of Reynolds stress detection only considering instrument noise as for the estimation of shear uncertainty (Williams and Simpson 2004). This uncertainty will be used in the estimation of TKE production uncertainty.

A comparison between the obtained Reynolds stresses from the five-beam profilers (after noise removal) and from direct covariance with the TTM ADV at Admiralty Inlet are shown in the scatterplot of Fig. 7. Blue and red dots are averages binned by $\overline{u'_{ch}w'}$ from the TTM ADV measurements. Despite large scatter in the comparison, the binned results are in agreement at higher Reynolds stresses. The large differences might be explained by the separation of the instruments and by the remaining noise in the Reynolds stress estimates.

Figures 8 and 9 show time series of vertical profiles of the five Reynolds stresses estimated following the R. Dewey and S. Stringer (2007, unpublished manuscript) method at Admiralty Inlet and Rich Passage, respectively. The horizontal Reynolds stresses ($\overline{u'^2_{ch}}$, $\overline{v'^2_{ch}}$) reach values that are an order of magnitude higher than the rest of the estimated Reynolds stresses at both sites. The magnitude of the Reynolds stresses is modulated by the tidal currents. At Admiralty Inlet, the Reynolds

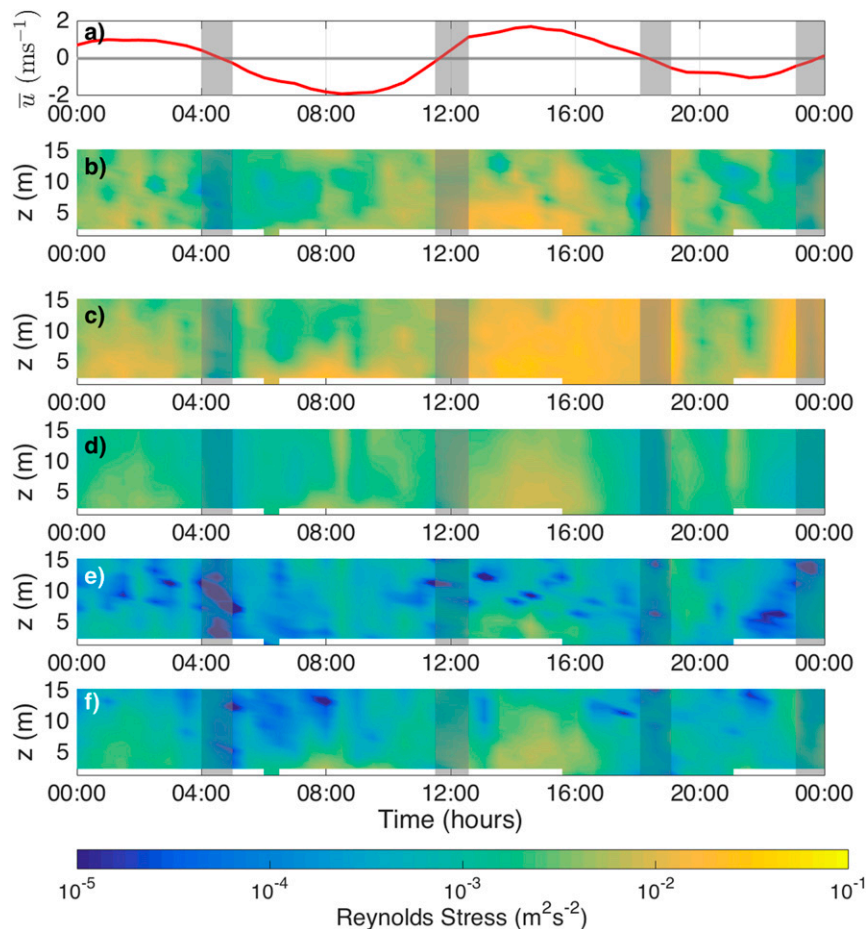


FIG. 9. Horizontal burst-averaged speed and vertical profiles of Reynolds stresses in time estimated using R. Dewey and S. Stringer (2007, unpublished manuscript) five-beam method at Rich Passage: (a) mean flow, (b) $\overline{u_{ch}^2}$, (c) $\overline{v_{ch}^2}$, (d) $\overline{w^2}$, (e) $\overline{u_{ch} w'}$, and (f) $\overline{v_{ch} w'}$. Slack conditions are marked in gray.

stresses' magnitude increases as the horizontal speed increases, and the maximum values are observed during the observed ebb. At Rich Passage (Fig. 9), the Reynolds stresses' magnitude also increases with the horizontal speed. The highest Reynolds stresses are observed during the highest flood tidal current.

Figure 10 shows vertical profiles of the estimated vertical shear Reynolds stress ($\overline{u'_{ch} w'}$), averaged for ebb and flood at the two sites together with ADV estimates when available. Additionally, estimates using the variance technique with no tilt corrections for the two five-beam acoustic Doppler current profilers at both sites are included.

At Admiralty Inlet, during ebb, averaged estimates from the two instruments are in good agreement, and are also in good agreement with the TTM ADV estimates. For the first 15 m of the water column, the estimates from the Nortek Signature are higher than those from the RDI Sentinel V50. During flood, the RDI Sentinel V50 estimates are higher than those from the

Nortek Signature through the entire water column. During ebb, the estimates from the variance technique are biased low during the lower portion of the water column and they are higher during the second portion of it. During flood, the variance technique estimates remain lower for most of the water column. This difference highlights the importance of the tilt corrections incorporated into the new calculations of the Reynolds stresses as previously reported by Lu and Lueck (1999).

At Rich Passage the two methods are in good agreement, with slightly lower estimates from the variance technique through the water column. However, the average estimate from the TT ADV at this site is much higher, which might be explained by motion contamination at low frequencies in u'_{ch} (Kilcher et al. 2017).

c. Vertical shear TKE production

The estimated Reynolds stresses together with the vertical shear are used to estimate the vertical shear

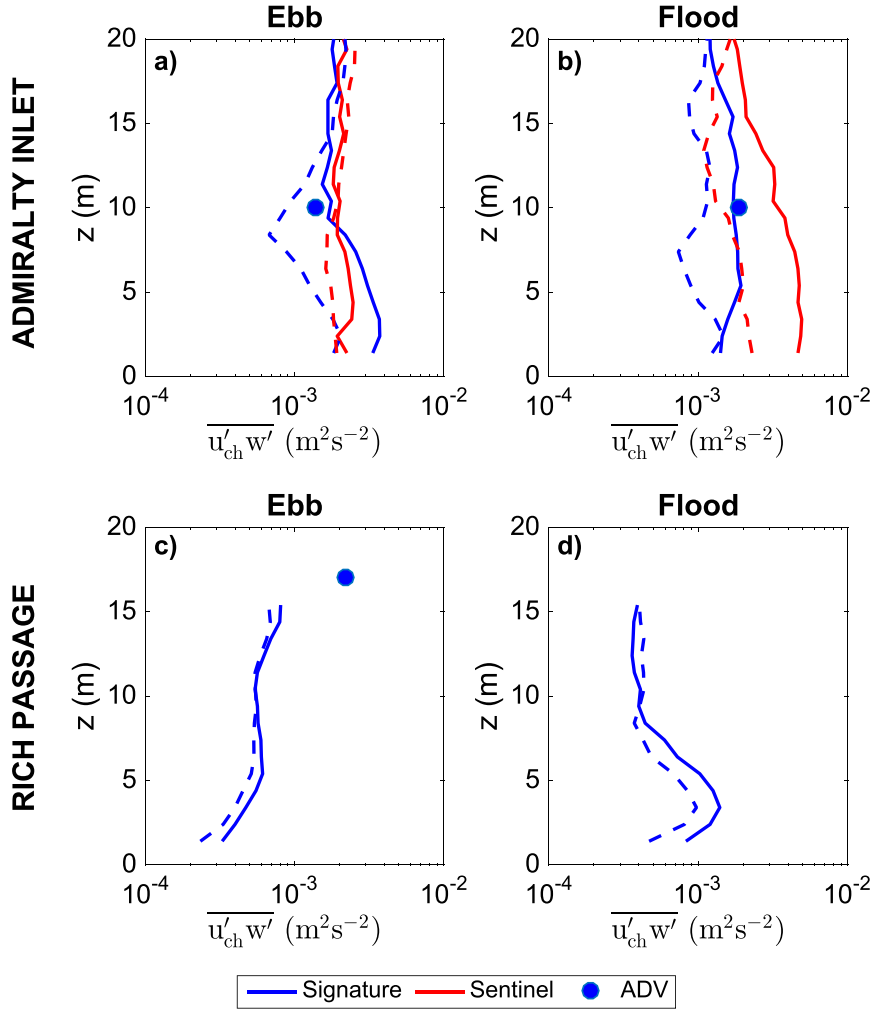


FIG. 10. Average vertical shear Reynolds stress ($\overline{u'_{ch} w'}$) profiles estimated using R. Dewey and S. Stringer (2007, unpublished manuscript) five-beam method at (a), (b) Admiralty Inlet and (c),(d) Rich Passage from the Nortek Signature data (blue) and RDI Sentinel V50 data (red). Estimates using the original variance technique with no tilt corrections (dashed lines; Stacey et al. 1999). Estimates from the ADV data (blue dots).

TKE production rate. The uncertainty in the TKE production estimations is calculated following the Williams and Simpson (2004) method, which is based on the variance of the product of two variables as follows:

$$\sigma_{P_{ij}}^2 = \overline{u'_i u'_j}^2 \sigma_S^2 + \frac{\partial \overline{u'_i}}{\partial x_j} \sigma_{RS}^2 + \sigma_S^2 \sigma_{RS}^2, \quad (14)$$

where $\sigma_{P_{ij}}$ is the uncertainty associated with the TKE production generated by the Reynolds stress $\overline{u'_i u'_j}$ and the shear $\partial \overline{u'_i} / \partial x_j$. Then the uncertainty of the vertical shear production P [Eq. (6)] is estimated as

$$\sigma_P = \sqrt{\sigma_{P_{uchw}}^2 + \sigma_{P_{vchw}}^2 + \sigma_{P_{ww}}^2}. \quad (15)$$

The averaged vertical profiles of TKE production for both sites separated by ebb and flood tides and their respective uncertainty are shown below (Fig. 12). In these plots, TKE production decreases with z , as expected for bottom-generated turbulence. The uncertainty in the TKE production increases with z , because $\sigma_{P_{ww}}$, which is the dominating term in the production uncertainty, increases with z . The $\sigma_{P_{ww}}$ uncertainty is dominated by its first term, $\overline{w' w'} \sigma_S^2$, which increases with z , as would be expected as vertical fluctuations grow toward the midwater column, as the distance from the boundary increases. At Admiralty Inlet, TKE production uncertainties range from 2% closer to the bottom, up to 90% at the top of the measured profile during ebb (26% maximum uncertainty during flood).

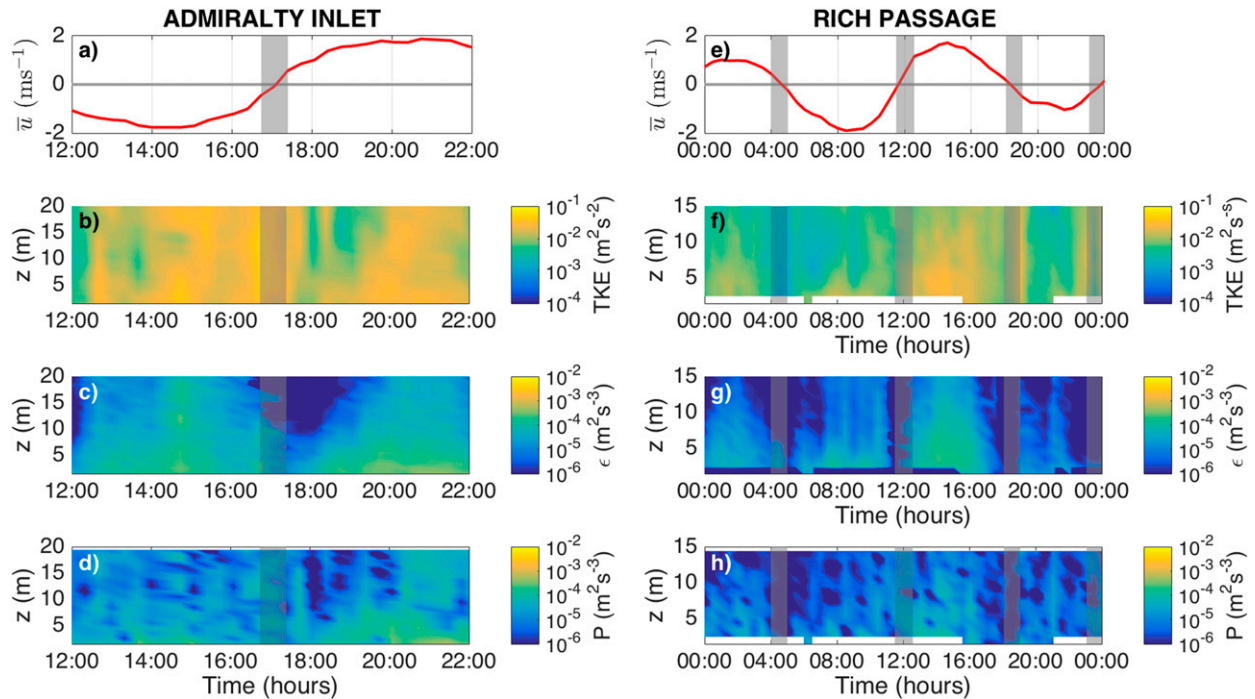


FIG. 11. Vertical profiles of TKE dissipation and production rates in time at (left) Admiralty Inlet and (right) Rich Passage. (a),(e) Mean horizontal speed; (b),(f) total TKE; (c),(g) TKE dissipation rate; (d),(h) TKE production rate.

At Rich Passage, uncertainties range from 6% closer to the bottom, up to 90% at the top of the measured profile.

5. Turbulent kinetic energy balance

The analysis of the turbulent kinetic energy balance from field measurements usually assumes that TKE production balances TKE dissipation. The inclusion of the fifth beam in these new acoustic current Doppler profilers allows for an improved estimation of TKE production; hence, a better closure of the TKE balance is possible. This improved TKE balance might indicate that other terms in the TKE balance, such as the TKE transport, are of importance, and it can be used to improve turbulence closure models in these environments.

Assuming that the buoyancy term is negligible at these well-mixed sites and that self-advection is small, the rate of change of TKE can be approximated as a local production–dissipation balance,

$$\frac{D}{Dt}(\text{TKE}) \approx P - \varepsilon. \quad (16)$$

Figure 11 shows the burst-averaged horizontal speed and vertical profiles in time of total TKE, TKE dissipation rate (from spectra), and TKE vertical production from the Nortek Signature data at both sites. At Admiralty Inlet, all three variables seem to be modulated

by the stage of the tidal current, increasing as the velocity magnitude increases; however, larger TKE, and TKE dissipation and production rates are observed during ebb. A similar pattern is observed at Rich Passage, where the variables are also modulated by the tidal currents but larger values are observed during the stronger flood.

Figure 12 shows an approximate TKE budget as depth profiles of vertical shear TKE production and TKE dissipation rates from the Nortek Signature data. Rates are averaged over all burst-averaged horizontal speeds, for ebb and flood at each site. The expected balance is generally found; however, there are distinct patterns that likely are related to the lateral headland at Admiralty Inlet and the vertical sill at Rich Passage.

During ebb at Admiralty Inlet, TKE production exceeds dissipation closer to the bottom and then an approximate balance is observed above $z = 10.4$ m. During flood, production and dissipation are approximately balanced up to $z = 15.4$ m, and production exceeds dissipation in the higher portion of the water column. At Rich Passage, production is balanced by dissipation for most of the water column during ebb, except below $z = 5.4$ m, where dissipation exceeds production. During flood, dissipation exceeds production throughout the entire profile.

Figure 13 shows scatterplots of TKE production versus TKE dissipation rates for all burst-averaged velocities

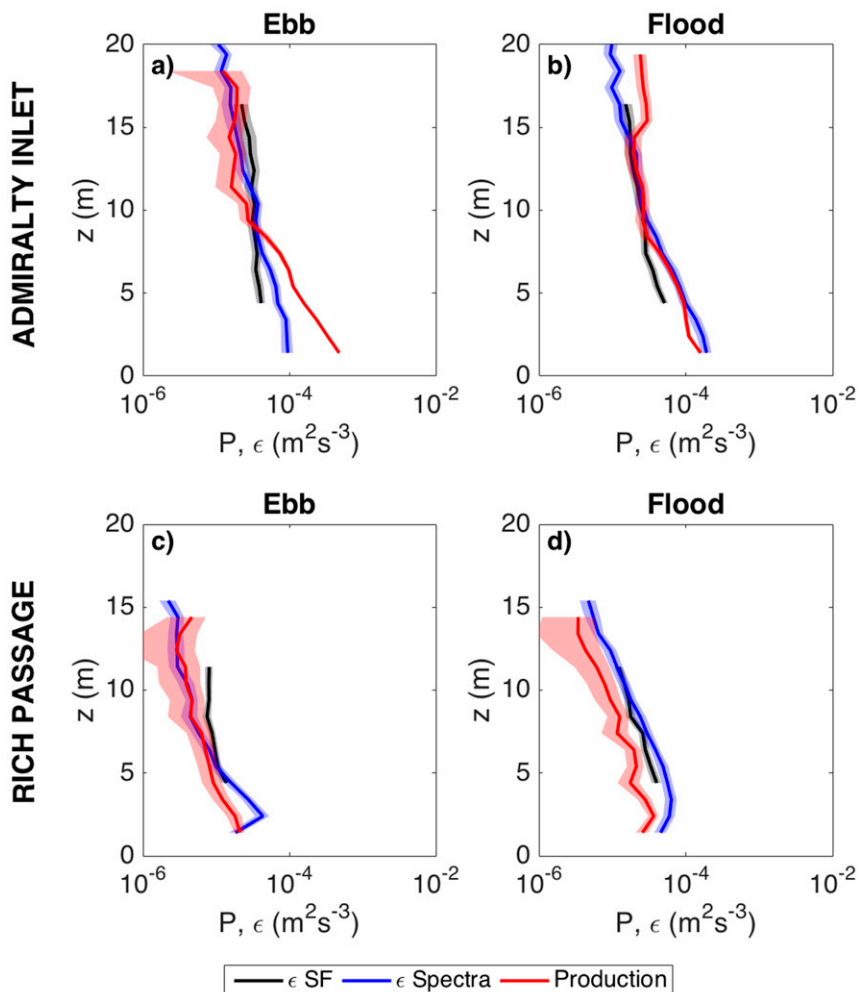


FIG. 12. An approximate TKE budget shown using average TKE dissipation rates from the two methods and TKE shear production from Reynolds stresses from the Nortek Signature data at (a),(b) Admiralty Inlet and (c),(d) Rich Passage.

and all depths. The values are well correlated over several orders of magnitude, albeit with significant scatter. At Admiralty Inlet, a near 1:1 balance between TKE production and TKE dissipation during the most energetic conditions is observed. During less energetic conditions, TKE production exceeds TKE dissipation, suggesting that the transport of turbulent kinetic energy is of importance during such conditions. At Rich Passage, a near 1:1 balance between TKE production and TKE dissipation is observed during all conditions.

6. Conclusions

Two new five-beam acoustic current profilers—the Nortek Signature1000 (kHz) AD2CP and the RDI Sentinel V50—are successfully used to measure turbulence at two energetic tidal channels: Admiralty Inlet

and Rich Passage (Puget Sound, Washington). Turbulent kinetic energy (TKE) production and dissipation rates are estimated from the measurements, and an approximate TKE budget is obtained.

The results illustrate the capabilities of five-beam profilers for assessing high-order turbulence parameters. The TKE frequency spectra from the Nortek Signature presents a low noise level of $O(10^{-4})m^2s^{-2}$, while the RDI Sentinel V50 presents a higher noise level of $O(10^{-2})m^2s^{-2}$, comparable to the previous generation of profilers.

The lower noise observed on the Nortek Signature spectra might be attributed to its ability to sample faster (8 Hz when using all five beams); however, when subsampling the Nortek Signature data to 2 Hz (the maximum possible with the RDI), the noise level in the TKE spectra remains at $O(10^{-4})m^2s^{-2}$. The TKE spectra

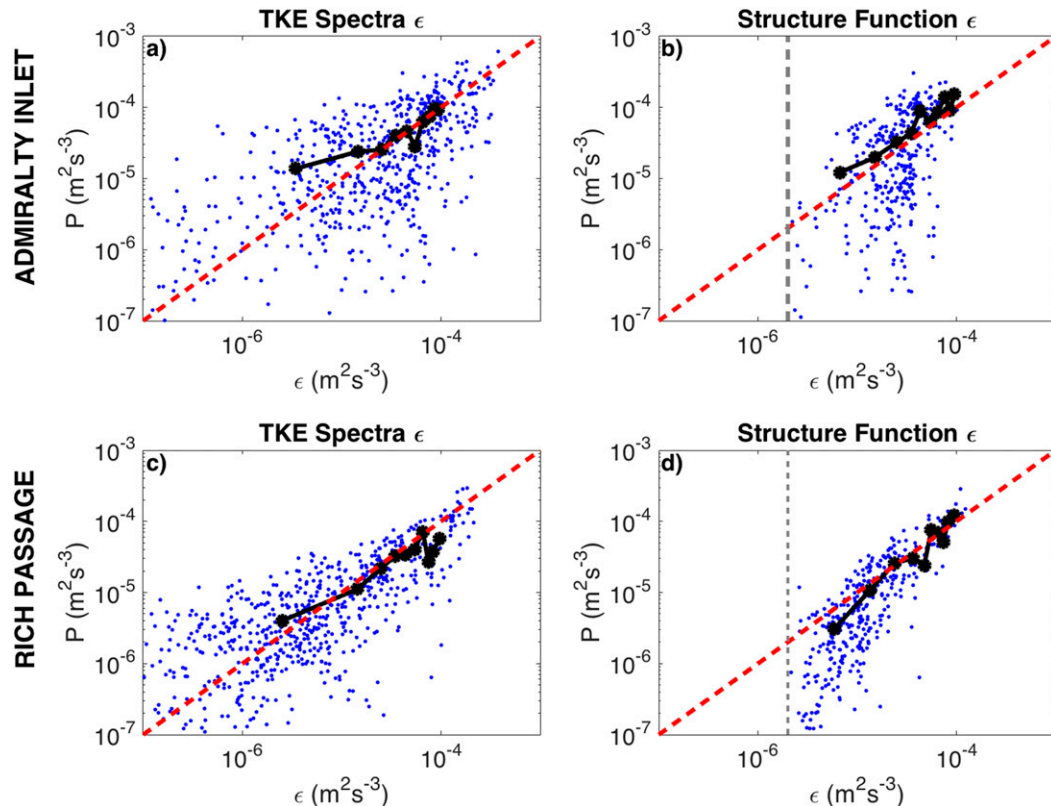


FIG. 13. TKE dissipation rate and TKE production for all \bar{u} and all depths at (a),(b) Admiralty Inlet and (b),(c) Rich Passage. Mean values of dissipation and production binned by dissipation (black dots); $y = x$ (red dashed line). Shown in (b),(d) is the limit of TKE dissipation detection when using the turbulence structure function (dashed gray line).

obtained with the Nortek Signature are in agreement with spectra from ADV measurements at both sites.

The lower noise level of the Nortek Signature enables observation of the inertial subrange of turbulence, and thus improved estimations of the TKE dissipation rate from both, TKE spectra and second-order structure function of turbulence. TKE dissipation rates from the two methods agree well with each other through the water column, and also with estimates from ADV data.

Although the TKE spectra from the RDI Sentinel V50 does not allow the observation of the inertial subrange, the lower-frequency portion of the spectra is well resolved and in agreement with the estimates from the Nortek Signature and the Nortek Vector. The RDI Sentinel V50 data can be used to estimate a synthetic vertical TKE spectrum using non-dimensional Kaimal curves (Kaimal et al. 1972). These curves can be fit to the lower portion of the TKE spectra and then used to extend the inertial subrange, and subsequently estimate the TKE dissipation rate. However, the derivation of the Kaimal

curves is based on a balance between TKE production and dissipation; thus, their application might only be appropriate at all depths were an approximate production–dissipation balance is observed in the studied sites (Walter et al. 2011).

The use of all five beams enables the direct estimation of five out of six of the Reynolds stresses, which allows for improved estimations of the TKE production rate and provides better information for developing and validating turbulence closure models. The new Reynolds stresses calculations include tilt corrections following the R. Dewey and S. Stringer (2007, unpublished manuscript) method. At Admiralty Inlet, Reynolds stresses estimates from the two profiling instruments are in agreement with estimates from ADV at higher Reynolds stresses. The small differences may be attributed to instrument separation and the remaining noise in the Reynolds stresses estimations.

The TKE dissipation rates and TKE production rates are used to analyze an approximate TKE budget at Admiralty Inlet and Rich Passage. In general, the

expected balance is observed; however, distinct patterns are observed at the two sites, which are thought to be related to bathymetric features that promote TKE advection and transport.

The most recent version of the Nortek Signature1000 includes an integrated motion unit, which enables instrument motion corrections, such that the instrument can also be mounted in buoys and/or moorings. The new firmware version of the Nortek Signature supports high-resolution (HR) measurements, enabling high-sampling frequency measurements in velocity bins as small as 0.02 m. The low Doppler noise of the Nortek Signature, similar to ADV noise levels, makes it even suitable for lower turbulence environments. ADVs have been successfully used to estimate TKE dissipation rates from TKE spectra in low turbulence environments, such as lakes in Brand et al. (2008) and Vachon et al. (2010).

The turbulence parameters that can be obtained with these new instruments are useful for the development and improvement of turbulence models, for the study of mixing processes, and for predicting sediment transport. The methods presented in this paper are implemented in MATLAB and are available through the MATLAB File Exchange website as five-beam acoustic Doppler current profiler turbulence methods (<http://www.mathworks.com/matlabcentral/fileexchange/57551-mguerrap-5beam-turbulence-methods>).

Acknowledgments. We thank Joe Talbert and Alex de Klerk for deployment and recovery of the instruments, and Andy Reay-Ellers for ship operations. We thank Levi Kilcher and Sam Harding for motion-corrected ADV data (used for validation). Funding was provided by NAVFAC (N00024-10-D-63). Maricarmen Guerra thanks the Fulbright (15140888) and the CONICYT Becas Chile doctorate fellowship programs.

REFERENCES

- Bassett, C., J. Thomson, and B. Polagye, 2013: Sediment-generated noise and bed stress in a tidal channel. *J. Geophys. Res. Oceans*, **118**, 2249–2265, doi:10.1002/jgrc.20169.
- Brand, A., D. McGinnis, B. Wehrli, and A. West, 2008: Intermittent oxygen flux from the interior into the bottom boundary of lakes as observed by eddy correlation. *Limnol. Oceanogr.*, **53**, 1997–2006, doi:10.4319/lo.2008.53.5.1997.
- Brumley, B., R. Cabrera, K. Deines, and E. Terray, 1991: Performance of a broad-band acoustics Doppler current profiler. *IEEE J. Oceanic Eng.*, **16**, 402–407, doi:10.1109/48.90905.
- Durgesh, V., J. Thomson, M. Richmond, and B. Polagye, 2014: Noise correction of turbulent spectra obtained from acoustic Doppler velocimeters. *Flow Meas. Instrum.*, **37**, 29–41, doi:10.1016/j.flowmeasinst.2014.03.001.
- Harding, S., L. Kilcher, and J. Thomson, 2017: Turbulence measurements from compliant moorings. Part I: Motion characterization. *J. Atmos. Oceanic Technol.*, **34**, 1235–1247, doi:10.1175/JTECH-D-16-0189.1.
- Kaimal, J., J. Wyngaard, Y. Izumi, and O. Coté, 1972: Spectral characteristics of surface-layer turbulence. *Quart. J. Roy. Meteor. Soc.*, **98**, 563–589, doi:10.1002/qj.49709841707.
- Kilcher, L., S. Harding, J. Thomson, and S. Nylund, 2017: Turbulence measurements from compliant moorings. Part II: Motion correction. *J. Atmos. Oceanic Technol.*, **34**, 1249–1266, doi:10.1175/JTECH-D-16-0213.1.
- Kolmogorov, A. N., 1941: Dissipation of energy in the locally isotropic turbulence. *Dokl. Akad. Nauk SSR*, **30**, 301–305.
- Lu, Y., and R. Lueck, 1999: Using a broadband ADCP in a tidal channel. Part II: Turbulence. *J. Atmos. Oceanic Technol.*, **16**, 1568–1579, doi:10.1175/1520-0426(1999)016<1568:UABAIA>2.0.CO;2.
- Lumley, J., and E. Terray, 1983: Kinematics of turbulence convected by a random wave field. *J. Phys. Oceanogr.*, **13**, 2000–2007, doi:10.1175/1520-0485(1983)013<2000:KOTCBA>2.0.CO;2.
- McCaffrey, K., B. Fox-Kemper, P. Hamlington, and J. Thomson, 2015: Characterization of turbulence anisotropy, coherence, and intermittency at a prospective tidal energy site: Observational data analysis. *Renewable Energy*, **76**, 441–453, doi:10.1016/j.renene.2014.11.063.
- McMillan, J., and A. Hay, 2017: Spectral and structure function estimates of turbulence dissipation rates in a high-flow tidal channel using broadband ADCPs. *J. Atmos. Oceanic Technol.*, **34**, 5–20, doi:10.1175/JTECH-D-16-0131.1.
- , —, R. Lueck, and F. Wolk, 2016: Rates of dissipation of turbulent kinetic energy in a high Reynolds number tidal channel. *J. Atmos. Oceanic Technol.*, **33**, 817–837, doi:10.1175/JTECH-D-15-0167.1.
- Pope, S. B., 2000: *Turbulent Flows*. Cambridge University Press, 802 pp.
- Richard, J., J. Thomson, B. Polagye, and J. Bard, 2013: Method for identification of Doppler noise levels in turbulent flow measurements dedicated to tidal energy. *Int. J. Marine Energy*, **3–4**, 52–64, doi:10.1016/j.ijome.2013.11.005.
- Rippeth, T., J. Simpson, E. Williams, and M. Inall, 2003: Measurement of the rates of production and dissipation of turbulent kinetic energy in an energetic tidal flow: Red wharf bay revisited. *J. Phys. Oceanogr.*, **33**, 1889–1901, doi:10.1175/1520-0485(2003)033<1889:MOTROP>2.0.CO;2.
- Rusello, P., and E. Cowen, 2011: Turbulent dissipation estimates from pulse coherent Doppler instruments. *2011 IEEE/OES/CWTM: Tenth Working Conference on Current, Waves and Turbulence Measurements (CWTM)*, J. Rizoli White and A. J. Williams III, Eds., IEEE, 167–172, doi:10.1109/CWTM.2011.5759546.
- Sreenivasan, K., 1995: On the universality of the Kolmogorov constant. *Phys. Fluids*, **7**, 2778–2784, doi:10.1063/1.868656.
- Stacey, M., S. Monismith, and J. Burau, 1999: Measurements of Reynolds stress profiles in unstratified tidal flow. *J. Geophys. Res.*, **104**, 10 933–10 949, doi:10.1029/1998JC900095.
- Thomson, J., 2012: Wave breaking dissipation observed with swift drifters. *J. Atmos. Oceanic Technol.*, **29**, 1866–1882, doi:10.1175/JTECH-D-12-00018.1.
- , B. Polagye, V. Durgesh, and M. Richmond, 2012: Measurements of turbulence at two tidal energy sites in Puget Sound, WA. *IEEE J. Oceanic Eng.*, **37**, 363–374, doi:10.1109/JOE.2012.2191656.
- , L. Kilcher, M. Richmond, J. Talbert, A. de Klerk, B. Polagye, M. Guerra, and R. Cienfuegos, 2013: Tidal turbulence spectra

- from a compliant mooring. *Proc. First Marine Energy Technology Symp. (METS2013)*, Washington, DC, Foundation for Ocean Renewables, 9 pp.
- Vachon, D., Y. Prairie, and J. Cole, 2010: The relationship between near-surface turbulence and gas transfer velocity in freshwater systems and its implications for floating chamber measurements of gas exchange. *Limnol. Oceanogr.*, **55**, 1723–1732, doi:[10.4319/lo.2010.55.4.1723](https://doi.org/10.4319/lo.2010.55.4.1723).
- Walter, R., N. Nidzieko, and S. Monismith, 2011: Similarity scaling of turbulence spectra and cospectra in a shallow tidal flow. *J. Geophys. Res.*, **116**, C10019, doi:[10.1029/2011JC007144](https://doi.org/10.1029/2011JC007144).
- Wiles, P., T. Rippeth, H. J. Simpson, and P. Hendricks, 2006: A novel technique for measuring the rate of turbulent dissipation in the marine environment. *Geophys. Res. Lett.*, **33**, L21608, doi:[10.1029/2006GL027050](https://doi.org/10.1029/2006GL027050).
- Williams, E., and J. Simpson, 2004: Uncertainties in estimates of Reynolds stress and TKE production rate using the ADCP variance method. *J. Atmos. Oceanic Technol.*, **21**, 347–357, doi:[10.1175/1520-0426\(2004\)021<0347:UIEORS>2.0.CO;2](https://doi.org/10.1175/1520-0426(2004)021<0347:UIEORS>2.0.CO;2).